nature photonics

ARTICLES

PUBLISHED ONLINE: 22 MARCH 2009 | DOI: 10.1038/NPHOTON.2009.26

Heat-assisted magnetic recording by a near-field transducer with efficient optical energy transfer

W. A. Challener*, Chubing Peng, A. V. Itagi, D. Karns, Wei Peng, Yingguo Peng, XiaoMin Yang, Xiaobin Zhu, N. J. Gokemeijer, Y.-T. Hsia, G. Ju, Robert E. Rottmayer, Michael A. Seigler and E. C. Gage

Although near-field microscopy has allowed optical imaging with sub-20 nm resolution, the optical throughput of this technique is notoriously small. As a result, applications such as optical data storage have been impractical. However, with an optimized near-field transducer design, we show that optical energy can be transferred efficiently to a lossy metallic medium and yet remain confined in a spot that is much smaller than the diffraction limit. Such a transducer was integrated into a recording head and flown over a magnetic recording medium on a rotating disk. Optical power from a semiconductor laser at a wavelength of 830 nm was efficiently coupled by the transducer into the medium to heat a 70-nm track above the Curie point in nanoseconds and record data at an areal density of ~375 Tb m^{-2}. This transducer design should scale to even smaller optical spots.

Light can be focused by conventional far-field optics to a spot that is limited by diffraction to ~0.5 λ/NA where λ is the wavelength and NA is the numerical aperture of the lens. The near-field scanning optical microscope[1], on the other hand, can achieve a resolution of 100 nm or better. Near-field microscopy typically uses either tapered optical fibres or hollow silicon cantilevers with a very small aperture that is scanned across the sample, but the optical throughput[2,3] is in the order of 1×10^{-4} to 1×10^{-5}. Using concentric grooves around an aperture in an aluminium film can substantially enhance the throughput; this has recently been used to expose marks in photoresist with a linewidth of 80 nm (ref. 4). Apertureless microscopy has achieved sub-20-nm optical resolution[5] by focusing a laser beam onto a sharp metallic tip, which concentrates the optical field onto the sample.

The storage density of hard disk drives has doubled every three years since their introduction in 1955. Several major technology advances, including the development of thin-film media and recording heads, giant magnetoresistive readers, and perpendicular recording, have enabled the current areal density of 750 Tb m^{-2}, which is about half the theoretical limit for conventional magnetic recording materials. As the magnetic grain size is reduced to increase the storage density, the grains may become superparamagnetic and their magnetic state thermally unstable[6]. Materials with a large magnetic anisotropy, such as $L1_0$ FePt (ref. 7), can support grains as small as 2 to 3 nm in diameter and storage densities[8] up to 155 Pb m^{-2}. However, the coercivity of high-anisotropy materials is greater than the magnetic field that can be generated by a recording head.

Heat-assisted magnetic recording (HAMR) overcomes this problem by heating the medium above its Curie point during recording to reduce its coercivity to zero[8]. Optical energy must be efficiently delivered and confined to a spot in the medium that is much smaller than the diffraction limit so that neighbouring tracks are not heated. Heating and cooling of the medium must occur within ~1 ns in order to achieve the necessary data rates, to generate a large thermal gradient for sharp bit edge definition, and to ensure that the recorded data are thermally stable during cooling to ambient.

A planar solid immersion mirror (PSIM) is a parabolically shaped waveguide with a NA much larger than 1 that can focus light to ~λ/4 (ref. 9). HAMR has been demonstrated with PSIMs in integrated recording heads at storage densities of ~230 Tb m^{-2} at a wavelength of 488 nm (refs 10 and 11), and at densities of ~80 Tb m^{-2} at a wavelength of 830 nm. Nevertheless, much smaller optical spots are necessary for HAMR to exceed the current storage densities.

Results

The near-field transducer. Surface plasmons (SPs) are collective oscillations of surface charge that are confined to an interface between a dielectric and a metal. When SPs are resonantly excited by an external optical field, the field amplitude in the vicinity of the surface may be orders of magnitude greater than that of the incident field. Moreover, the region of enhanced field may be tightly confined to a spot much smaller than the incident wavelength. Gold is a suitable plasmonic material for wavelengths longer than ~700 nm as it is chemically inert with a relatively high melting point. At shorter wavelengths the electronic *d*-band transitions damp the SP effect.

A gold near-field transducer (NFT) that is excited at a SP resonance can couple light even more efficiently into a nearby medium by including a sharp tip in its design to take advantage of the lightning rod effect[12,13]. The electric field can also be enhanced in a narrow gap between two resonant nanoparticles[14,15]. A NFT design[16] that combines these enhancement mechanisms is shown in Figs 1a and 4a and is called a 'lollipop' transducer for obvious reasons. The NFT is located at the focus of a PSIM as shown in Fig. 1b, and at resonance the surface charge oscillates along the length of the lollipop peg to generate an electric field at the tip of the peg that couples energy into the medium. The peg provides the lightning rod effect for field confinement. A plasmonic metal beneath the recording layer acts as both a heat sink and an image plane for the electric field. The recording layer is effectively within the gap of two nanoparticles, the NFT and its image, resulting in a substantial enhancement in coupling efficiency and further confinement of the electric field.

Seagate Technology, 1255 Waterfront Place, Pittsburgh, Pennsylvania 15222, USA. *e-mail: william.a.challener@seagate.com

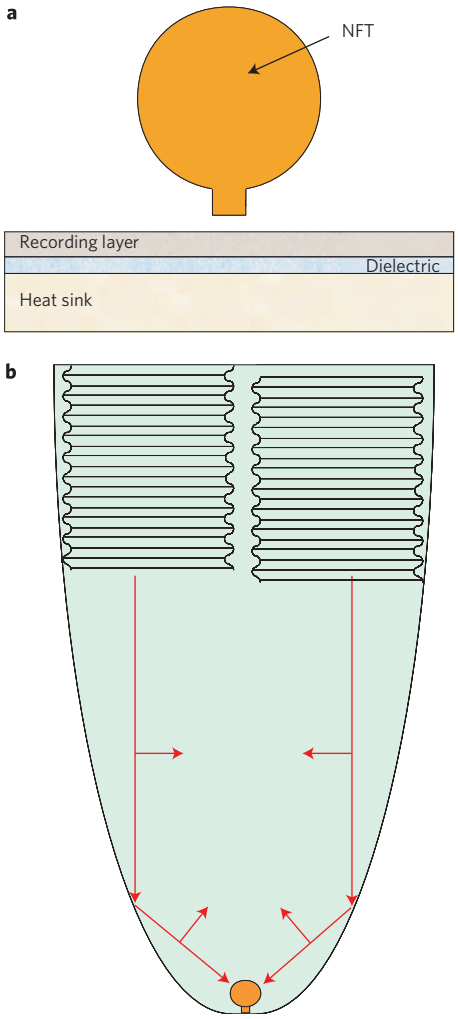

Figure 1 | Diagram of the NFT and its position in the PSIM. a, Expanded view of the NFT showing its vertical position with respect to the recording medium. The medium is modelled as 12.5 nm Fe, 5 nm MgO and 50 + nm Cu. The 7.5-nm gap between the NFT and the medium is modelled with an effective index slightly greater than air to include the effect of the lubricant and carbon overcoats. **b**, A planar solid immersion mirror with a dual offset grating used to focus a waveguide mode onto the lollipop NFT. The electric field for the TE mode is shown, which generates a longitudinal (vertical) field at the focus.

The incident light must be polarized along the vertical axis of the NFT to excite the proper SP resonance. The coupling grating at the top of the PSIM is divided into two halves that are vertically offset by half a period with respect to each other. There is a π-phase shift between the transverse electric (TE) waveguide modes launched on either side of the PSIM. When the modes combine at the focus, the net field is longitudinally polarized as shown in Fig. 1b. This grating/PSIM is the planar equivalent of radially polarized light, for which a longitudinal field is also obtained at the focus[17,18].

Theoretical optimization of the transducer. NFTs have been theoretically characterized in the literature in a variety of different ways. Because a metallic medium in proximity to a NFT can strongly affect its resonant behaviour, it is essential that the medium be included in the model. A NFT that exhibits a large field enhancement or throughput in free space may nevertheless perform quite poorly as a HAMR NFT[19]. An appropriate figure of merit (FOM) for theoretically optimizing the NFT design is the fraction of total incident focused optical power that is dissipated within a specific region of the medium. A 70 $\times$ 70 nm^2 region in the recording layer is chosen for our finite-difference time-domain (FDTD) simulations[20–22].

The lollipop NFT is a composite design obtained by combining a circular disk with a peg. The disk dimensions are optimized to function as an antenna for the incident light, resonating at the chosen wavelength while funnelling energy into the peg for confined transfer to the recording medium. The composite lollipop NFT is about four times more efficient than a straight peg NFT by itself.

A rather complex optimization process is required to find the size and position of the lollipop NFT within the waveguide that maximizes the FOM. The field intensity within the medium decays exponentially as the distance to the NFT increases (see Supplementary Fig. S1). The gap between the bottom of the NFT and the top of the recording layer for our simulations is 7.5 nm, consistent with read back signal requirements at storage densities of 1.5 Pb m^{-2} (1 Tb in^{-2}). The best coupling at a wavelength of 870 nm occurs for our waveguide when the NFT is placed about 20 nm outside the core. In this case, the peak field intensity in the gap is $\sim$2,000 times larger than that of the incident focused field intensity, as shown in Fig. 2c, and is $\sim$4% larger at the edges of the peg than under the centre of the peg. The peak FOM for a NFT that is 30 nm thick is $\sim$8%, as shown in Fig. 2a, and is orders of magnitude greater than the coupling efficiency of simple apertures with diameters of the same dimensions as the peg. The simulated field intensity in the centre layer of the recording medium, which is proportional to the dissipated power in the medium, is shown in Fig. 2b.

As the peg width is reduced, the optical spot size in the medium is also reduced and the peak field intensity within the medium increases. Therefore, this NFT should perform even better at higher storage densities and smaller optical spots.

In conventional disk drives the head-to-medium spacing is controlled by localized electrical heating of the recording head. This causes differential thermal expansion of the head (see Supplementary Fig. S2). In a HAMR head, the additional heat from absorbed laser light causes the NFT to protrude towards the surface of the disk during recording by several nanometres[8]. The protrusion increases the coupling efficiency, but it must be carefully controlled so that the NFT does not contact the disk surface. The surface roughness of the recording medium must also be sufficiently small not to cause significant variations in coupling efficiency.

The edge of a recorded mark occurs at that point on the track in the medium between the NFT and the recording pole for which the applied magnetic field equals the coercivity of the medium at the local temperature. Owing to the aggressive heat sinking of the medium, the mark edge is located closer to the NFT than to the recording pole. Therefore, the magnitude of the magnetic field at the recording position is smaller than the field at the edge of the pole. Reducing the spacing between the NFT and recording pole can increase the magnetic field within the hot spot, but this also reduces the NFT efficiency as the proximity of the lossy metallic pole damps the NFT resonance.

Fabrication of the recording head. An integrated recording head is shown in Fig. 3. The complete optical system includes two coupling gratings at the top of the device to insert a free-space laser beam into both sides of the PSIM waveguide, a PSIM to focus the TE waveguide mode onto the NFT, and the lollipop NFT itself. The input coupling grating has a groove depth of $\sim$60 nm with a period of 750 nm for efficiently coupling[23] of a 35-μm-diameter incident optical spot at a wavelength of 830 nm and an angle of incidence of 40°. A gold reflector beneath the lower cladding layer of the waveguide enhances the efficiency of the grating by reflecting the incident beam back to the grating for a second pass. The lower cladding thickness of 790 nm ensures the correct phase of the reflected beam at the grating. Approximately 50% of the

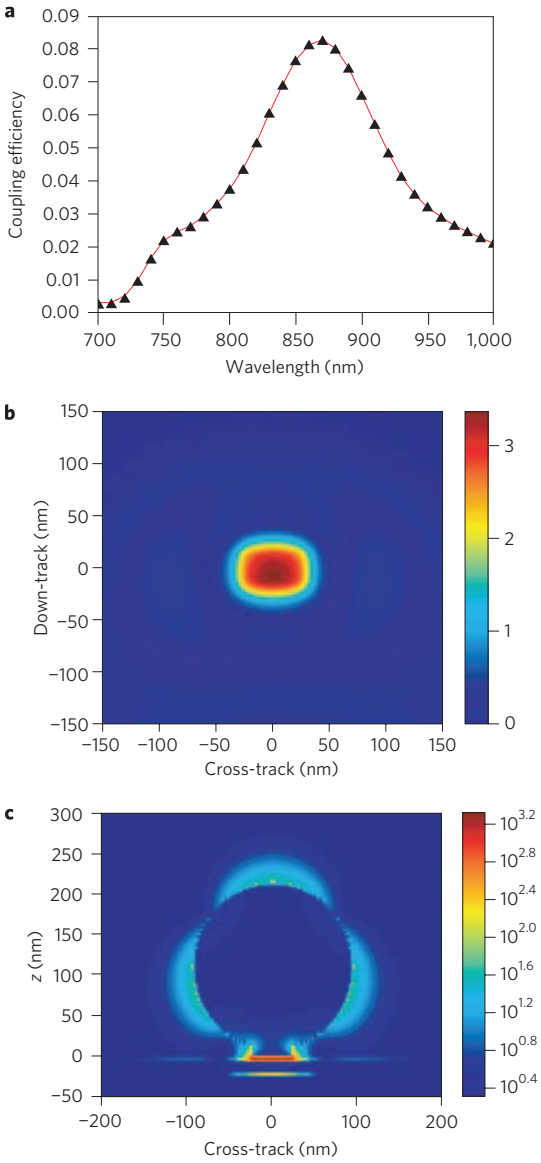

Figure 2 | NFT coupling efficiency and field intensity. a, Coupling efficiency of the lollipop NFT versus wavelength into a 70 × 70 nm^2 region of an Fe-like medium. **b**, Profile of $|E|^2$ field intensity within the centre of the recording layer at the resonance wavelength. **c**, Profile of the $|E|^2$ field intensity through a cross-section of the NFT.

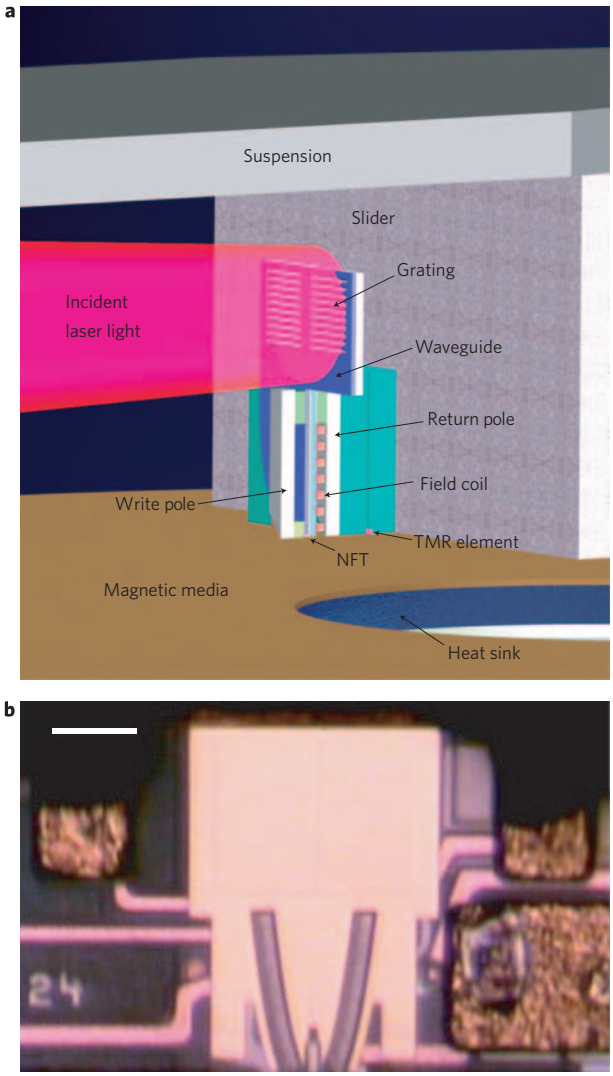

Figure 3 | Integrated recording head. a, Schematic of the integrated recording head incorporating the HAMR optics: a grating coupler, a PSIM waveguide and a lollipop NFT, as well as the magnetic components including the recording pole and TMR reader. **b**, Optical image of the recording head pressed against the glass slide. Scale bar, 50 μm.

incident light is coupled into the planar waveguide, which is composed of a 125-nm core of Ta_2O_5 with index 2.15, surrounded by an Al_2O_3 cladding with index 1.65. The effective index of the TE mode in the waveguide is 1.80. The diameter of the lollipop disk is ∼200 nm, the thickness of the disk and peg ∼22 nm, the length of the peg ∼15 nm and the width of the peg ∼50 nm. The imaginary part of the refractive indices for the waveguide layers must be less than $\sim 1 \times 10^{-5}$ to ensure minimal energy loss of the propagating beam.

The lollipop NFT was integrated with a recording pole and a tunnelling magnetoresistive reader on a recording head with a patterned air bearing surface designed so the head would fly over the surface of the magnetic recording disk rotating at 2,700 rpm or a linear speed of 7.2 m s^{-1}. The reader had a physical width of 55 nm. A lithographically defined gold lollipop NFT is shown in Fig. 4a and the air bearing surface of the recording head in the region of the NFT and recording pole is shown in Fig. 4b. The NFT-to-pole spacing was ∼40 nm. The width of the recording pole on the side next to the NFT was ∼310 nm. As seen in Fig. 4b, the peg of the NFT was not centred below the recording pole due to lithographic misalignments during fabrication, but the relatively large width of the recording pole ensures that the applied field is present in the region of the medium heated by the NFT.

Most of the NFT dimensions are determined by thin-film deposition or lithographic processes and can be controlled with high precision. The diameter of the disk in the lollipop or the refractive index of the surrounding dielectric can be reduced to shift the resonance to shorter wavelengths. The length of the peg of the lollipop is also affected by the lapping process and must be controlled to within ±10 nm to ensure an adequate coupling efficiency and optical spot size.

Fabrication of the recording medium

The recording medium was a 7.5-nm layer of FePt with a coercivity of 20.2 kOe, which was too large for a conventional perpendicular recording head to switch. Various underlayers were deposited on the substrate for epitaxial growth of the magnetic grains in the recording layer in the $L1_0$ crystalline structure. The medium did

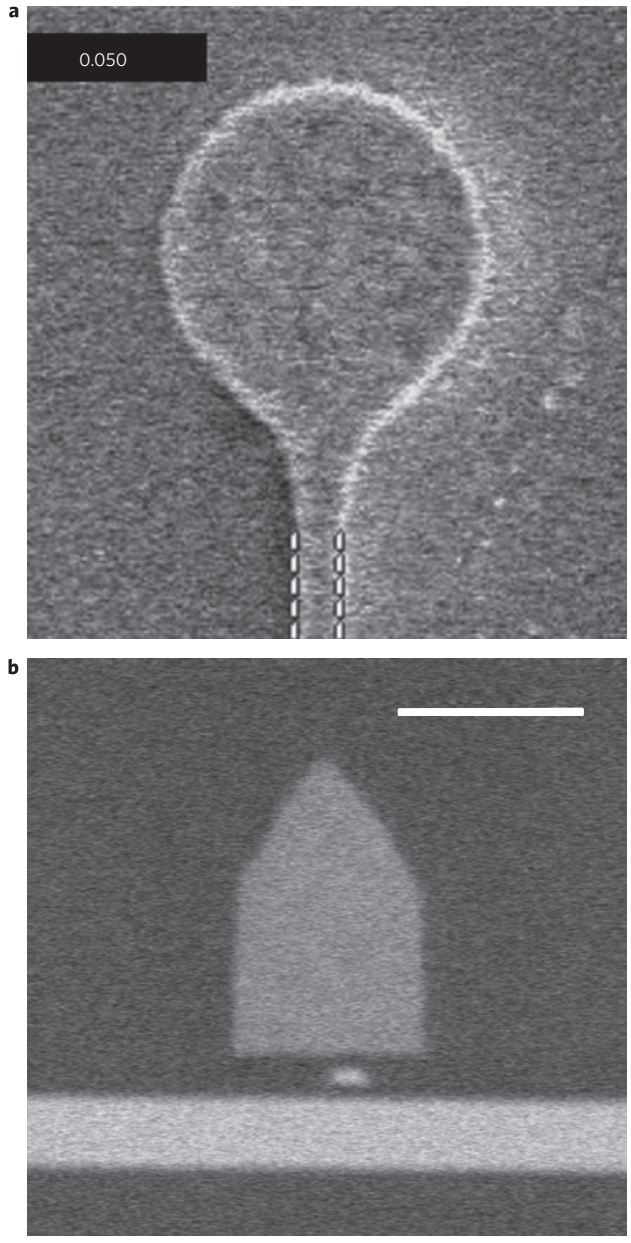

Figure 4 | SEM images of the NFT. a, SEM image of the gold lollipop NFT with a 50-nm peg width. The disk diameter in this image is ~350 nm. The distance between the dashed lines is 0.050 nm. **b**, SEM image of the NFT peg cross-section (small rectangle) and recording pole (trapezoid) from the air-bearing surface. The horizontal white band is the 125-nm Ta_2O_5 core. The peg width is ~60 nm and the thickness ~22 nm. Scale bar, 300 nm.

not incorporate a plasmonic image plane layer, thereby somewhat reducing the coupling efficiency, broadening the optical spot, and shifting the resonance peak to slightly shorter wavelengths from the modelled results. The surface of the disk had an r.m.s. roughness substantially less than 0.5 nm and was coated with a proprietary liquid lubricant with a decomposition temperature above 670 K.

Recording results. During recording, a constant 80 mW of laser power at a wavelength of 830 nm was incident upon the coupling grating, and the electrical heater current was adjusted to maintain a constant head-to-medium spacing of ~15 nm. This spacing corresponded to a physical air gap of ~2 nm between the bottom of the carbon overcoat on the recording head and the top of the lubricant on the disk. Differential thermal expansion from laser heating may have also caused a small protrusion of the NFT, reducing the NFT-to-medium spacing during recording as previously described. The coils around the recording pole were driven with 59 mA of current that was modulated at the data rate.

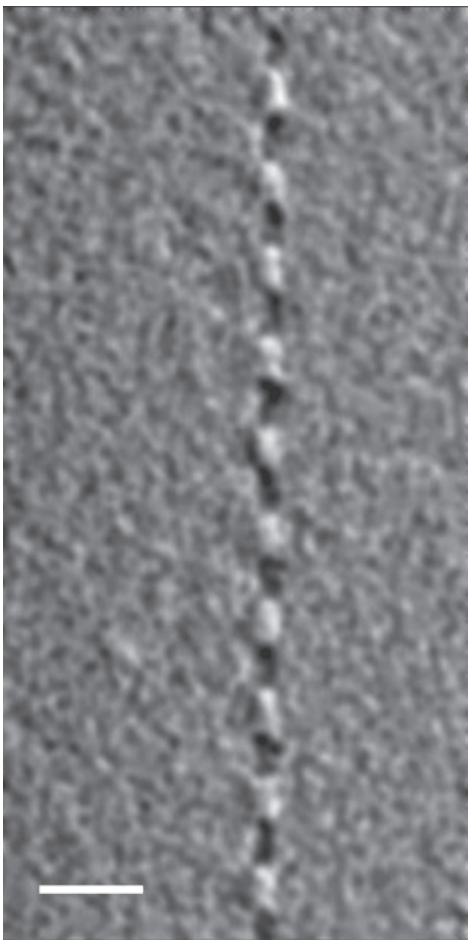

Figure 5 | MFM image of a recorded track. The track width is ~70 nm. Scale bar, 300 nm.

A magnetic force microscope (MFM) image of a recorded track is shown in Fig. 5. Because the recording layer is so thin, the magnetic field is very small and the image is rather noisy. The cross track signal for three adjacent recorded tracks with separations of 80 nm is shown in Fig. 6. An autocorrelated signal-to-noise ratio (ACSN) for a pseudo-random bit sequence, in which the background electronic noise was removed by averaging, was 15.5 dB for a full-width at half-maximum (FWHM) track width of 74 nm and a down track linear density of 36 nm per flux change. This track width is much smaller than the region of the medium that experiences the full applied magnetic field from the 310-nm-wide recording pole, and is consistent with a track squeeze experiment on a different head and recording medium as shown in Supplementary Fig. S3. In that experiment, the ACSN of a central recorded track was measured as neighbouring tracks were recorded on either side of it with varying offsets from the central track. Not until the track offset dropped below 80 nm was a sudden drop in ACSN measured. Therefore, it is reasonable to estimate an areal density of ~375 Tb m^{-2} for these HAMR results by multiplying the measured FWHM track width by the minimum bit length for which an acceptable signal-to-noise ratio of at least 15 dB was obtained.

The HAMR heads had lifetimes of up to several tens of track recordings. Thermal modelling indicates that the NFT temperature

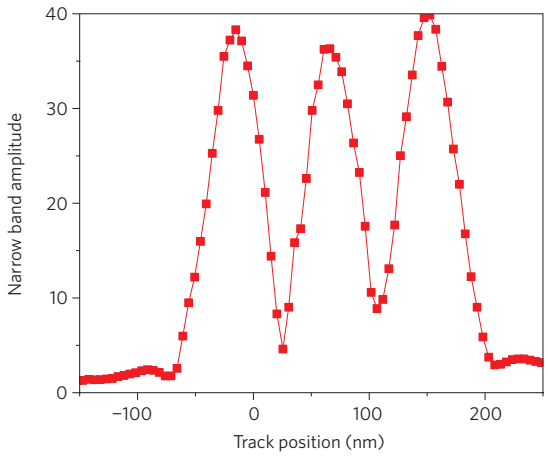

Figure 6 | Cross track scan of recorded data. Three tracks are recorded with an 80-nm offset.

may rise by several hundred degrees, but it remains well below the melting point of gold. The failure mode may be repeated thermal cycling of the NFT, the surrounding dielectrics and the recording medium. Appropriate materials engineering and thermal heat sinking can address this issue.

Discussion

A NFT has been designed that can efficiently couple optical energy into an absorptive medium in a region much smaller than the diffraction limit. The NFT has been demonstrated by incorporating it into a recording head to enable recording onto high-coercivity FePt media on a rotating disk. The recorded track width of ~70 nm was comparable to the width of the NFT peg and much narrower than either the recording pole or the wavelength of the incident laser beam, confirming the operation of the NFT. The Curie point of the medium was 650 K. Therefore, the medium was heated by ~350 °C or more within ~1 ns, evidence of the high coupling efficiency. The arrangement of the rotating disk at high speed with an air gap also confirms that there was no thermal transport by contact between the NFT and the medium. Future devices will include narrower pegs and additional optimization of both the NFT and the medium. It is estimated that the spot size can be reduced by up to 50% with improved coupling efficiency by including a copper heat sink in the recording medium. The gap between the NFT and the recording layer must also be reduced at higher storage densities to obtain a sufficient read back signal, and this smaller gap will significantly improve the efficiency of the NFT. Improving the thermal design of the recording medium and the coupling efficiency of the grating can also reduce the optical power required for recording, although the laser power used for this demonstration is already substantially less than that used in high-speed CD-R/RW disk drives. Other engineering challenges include thermal management of the head, lubricant and medium, acceptable process tolerances for high manufacturing yields, and further reduction in the magnetic grain size. However, these initial results show that it is possible to deliver optical energy to a metallic medium with relatively high efficiency in the near field confined to spot sizes an order of magnitude or more below the wavelength of light, and suggest that HAMR will provide the future technology for continued increases in magnetic disk drive storage density.

Received 1 September 2008; accepted 17 February 2009; published online 22 March 2009

References

1. Betzig, E., Trautman, J. K., Harris, T. D., Weiner, J. S. & Kostelak, R. L. Breaking the diffraction barrier: Optical microscopy on a nanometric scale. *Science* **251,** 1468–1470 (1991).
2. Ohtsu, M. & Hori, H. *Near-Field Nano-Optics* 129 (Kluwer, 1999).
3. Minh, P. N., Ono, T., Tanaka, S. & Esashi, M. High throughput aperture near-field scanning optical microscopy. *Rev. Sci. Instrum.* **71,** 3111–3117 (2000).
4. Srituravanich, W. *et al.* Flying plasmonic lens in the near field for high-speed nanolithography. *Nature Nanotech.* **3,** 733–737 (2008).
5. Sánchez, E. J., Novotny, L. & Xie, X. S. Near-field fluorescence microscopy based on two-photon excitation with metal tips. *Phys. Rev. Lett.* **82,** 4014–4017 (1999).
6. Lu, P. L. & Charap, S. H. Magnetic viscosity in high-density recording. *J. Appl. Phys.* **75,** 5768–5770 (1994).
7. Weller, D. & Moser, A. Thermal effect limits in ultrahigh-density magnetic recording. *IEEE Trans. Magn.* **35,** 4423–4439 (1999).
8. Kryder, M. H. *et al.* Heat assisted magnetic recording. *Proc. IEEE* **96,** 1810–1835 (2008).
9. Challener, W. A., Mihalcea, C., Peng, C. & Pelhos, K. Miniature planar solid immersion mirror with focused spot less than a quarter wavelength. *Opt. Exp.* **13,** 7189–7197 (2005).
10. Peng, C., Mihalcea, C., Büchel, D., Challener, W. A. & Gage, E. C. Near-field optical recording using a planar solid immersion mirror. *Appl. Phys. Lett.* **87,** 151105 (2005).
11. Seigler, M. A. *et al.* Heat assisted magnetic recording with a fully integrated recording head. *Proc. SPIE* **6620,** 66200P (2007).
12. Liao, P. F. & Wokaun, A. Lightning rod effect in surface enhanced Raman scattering. *J. Chem. Phys.* **76,** 751–752 (1982).
13. Martin, Y. C., Hamann, H. F. & Wickramasinghe, H. K. Strength of the electric field in apertureless near-field optical microscopy. *J. Appl. Phys.* **89,** 5774–5778 (2001).
14. Aravind, P. K., Nitzan, A. & Metiu, H. The interaction between electromagnetic resonances and its role in spectroscopic studies of molecules adsorbed on colloidal particles or metal spheres. *Surf. Sci.* **110,** 189–204 (1981).
15. Moskovits, M. Surface-enhanced spectroscopy. *Rev. Mod. Phys.* **57,** 783–826 (1985).
16. Challener, W. A. Transducer for heat assisted magnetic recording. US patent 7,272,079 (2007).
17. Quabis, S., Dorn, R., Eberler, M., Glöckl, O. & Leuchs, G. Focusing light to a tighter spot. *Opt. Commun.* **179,** 1–7 (2000).
18. Scully, M. O. & Zubairy, M. S. Simple laser accelerator: Optics and particle dynamics. *Phys. Rev. A* **44,** 2656–2663 (1991).
19. Challener, W. A., Gage, E., Itagi, A. & Peng, C. Optical transducers for near field recording. *Jpn J. Appl. Phys.* **45,** 6632–6642 (2006).
20. Taflove, A. & Hagness, S. C. *Computational Electrodynamics: the Finite-Difference Time-Domain Method* (Artech House, 2000).
21. Kunz, K. S. & Luebbers, R. J. *The Finite Difference Time Domain Method for Electromagnetics* (CRC Press, 1993).
22. Challener, W. A., Sendur, I. K. & Peng, C. Scattered field formulation of finite difference time domain for a focused light beam in dense media with lossy materials. *Opt. Exp.* **11,** 3160–3170 (2003).
23. Peng, C. & Challener, W. A. Input-grating couplers for narrow Gaussian beam: influence of groove depth. *Opt. Exp.* **12,** 6481–6490 (2004).

Acknowledgements

The authors would like to thank many colleagues at Seagate Research who supported this work, including C. Hardie, R. Hempstead, J. Keily, M. Kryder, L. Lee, C. Mihalcea, T. Morkved, K. Pelhos, T. Rausch, M. Re, K. Sendur and M. Xiao. Part of this work was performed under the INSIC HAMR ATP Program, with the support of the US Department of Commerce, National Institute of Standards and Technology, Advanced Technology Program, Cooperative Agreement Number 70NANB1H3056.

Additional information

Supplementary Information accompanies this paper at www.nature.com/naturephotonics. Reprints and permission information is available online at http://npg.nature.com/reprintsandpermissions/. Correspondence and requests for materials should be addressed to W.A.C.